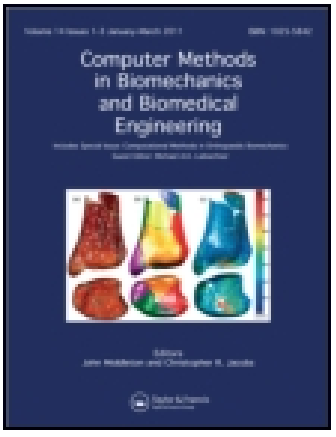

Computer Methods in Biomechanics and Biomedical Engineering
Publication details, including instructions for authors and subscription information:
http://www.tandfonline.com/loi/gcmb20

Modelling and simulation of substrate elasticity sensing in stem cells

Xiaowei Zeng [a] & Shaofan Li [a]
[a] Department of Civil and Environmental Engineering , University of California , Berkeley, CA, 94720, USA
Published online: 21 Apr 2011.

To cite this article: Xiaowei Zeng & Shaofan Li (2011) Modelling and simulation of substrate elasticity sensing in stem cells, Computer Methods in Biomechanics and Biomedical Engineering, 14:05, 447-458, DOI: 10.1080/10255842.2011.557371

To link to this article: http://dx.doi.org/10.1080/10255842.2011.557371

Computer Methods in Biomechanics and Biomedical Engineering
Vol. 14, No. 5, May 2011, 447–458

Taylor & Francis
Taylor & Francis Group

Modelling and simulation of substrate elasticity sensing in stem cells

Xiaowei Zeng and Shaofan Li*

Department of Civil and Environmental Engineering, University of California, Berkeley, CA 94720, USA

(*Received 31 July 2010; final version received 20 January 2011*)

Recently, we have developed a multiscale soft matter cell model aiming at improving the understanding of mechanotransduction mechanism of stem cells, which is responsible for information exchange between cells and their extracellular environment. In this paper, we report the preliminary results of our research on multiscale modelling and simulation of soft contact and adhesion of stem cells. The proposed multiscale soft matter cell model may be used to model soft contact and adhesion between cells and their extracellular substrates. To the authors' best knowledge, this may be the first time that a soft matter model has been developed for cell contact and adhesion. Moreover, we have developed and implemented a Lagrange-type meshfree Galerkin formulation and related computational algorithms for the proposed cell model. Comparison study with experimental data has been conducted to validate the parameters of the cell model. By using the soft matter cell model, we have simulated the soft adhesive contact process between cells and extracellular substrates. The simulation shows that the cell can sense substrate elasticity by responding it in different manners from cell spreading to cell contact configuration and molecular conformation changes.

Keywords: cell spreading; focal adhesion; hyperelasticity; liquid crystal; meshfree method; multiscale simulations

1. Introduction

Stem cells can sense and respond to physical signals during cell-to-cell or cell-extracellular matrix (ECM) interactions, and they can then integrate and process this information. Subsequently, these information or signals can trigger a host of reactions in stem cells, including changes of cell morphology, dynamics, genetic responses, overall behaviours and eventually their fate (Geiger et al. 2009).

Cell adhesion and spreading depend strongly on the interactions between cell and ECM substrates. When cultured onto artificial adhesive surfaces, cells first flatten and deform extensively as they spread (Cuvelier et al. 2007). Not all cell types respond to substrate stiffness in the same way, but many including endothelial cells (Yeung et al. 2005), mammary epithelial cells (Paszek et al. 2005) and mesenchymal stem cells (Engler et al. 2006) exhibit increased spreading and adhesion on stiffer substrates compared to compliant ones (Winer et al. 2009).

Recent developments on stem cell research have revealed that the fate or lineage specification of stem cells depends sensitively on both the rigidity and the surface microstructure of the ECM. For example, Discher et al. (2005) and Engler et al. (2006) reported that matrix elasticity directs stem cell lineage specification. Rehfelt et al. (2007) reported that the results with drug treatments of various cells on soft, stiff and rigid matrices show a broad range of possible matrix-dependent drug responses; and cells on soft gels might be relatively unaffected in cell spreading or apoptosis induction, whereas cells on stiff substrates seem more sensitive to diverse drugs in terms of spreading. All these indicate a significant influence of matrix elasticity on cell contact or adhesion, and subsequent cytoskeleton re-organisation.

Studying the influences of biomechanical niche factors on the fate of stem cells will eventually help in the development of synthetic niches that may cultivate or trigger stem cells to differentiate into the desirable functional cells (see Discher et al. 2009). Because of its scientific and clinical importance, a major focus of molecular cell biology is the study of mechanotransduction effect of cells, in particular stem cells (see Bao and Suresh 2003; Chien 2007; Wang et al. 2009).

Thus, understanding the interplay between cellular contractile activity, stiffness of surrounding tissues and the resulting mechanical deformations and stresses is crucial for establishing a mechanotransduction model. The physical process of mechanotransduction is through contact and adhesion between cells and their extracellular environment.

Recently, several general cell contact and focal adhesion models have been proposed, notably Freund and Lin (2004), Ni and Chiang (2007) and Deshpande et al. (2008). Continuum models have also been developed recently to predict cell adhesion in the early stages of culture (Liu et al. 2007; Sun et al. 2009) as well as to simulate cell motility (Roy and Qi 2010).

*Corresponding author. Email: shaofan@berkeley.edu

ISSN 1025-5842 print/ISSN 1476-8259 online

DOI: 10.1080/10255842.2011.557371
http://www.informaworld.com

In order to understand the precise biomechanical sensing process during cell contact and adhesion as well as to explain possible mechanotransduction mechanisms, we have developed the following multiscale cell model. In a recent paper (Zeng and Li 2011), the present authors have reported some early results of this effort. The main difference between this paper and Zeng and Li (2011) is as follows: in this paper, we not only discuss the substrate elasticity-induced configuration change in cell shape but also study the substrate elasticity-induced confirmation change in molecular structures, and most importantly we extend the cell model to three dimensions.

The paper is organised in six sections: in Section 2, we report the construction of our soft matter cell and ECM model; in Section 3, we focus on the meshfree implementation of the computational cell model; in Section 4, we discuss the cell adhesion and contact algorithm; in Section 5, we provide the validation of the cell model and a few numerical simulations and finally in Section 6, we discuss some important issues of the soft matter cell model.

2. Cell and ECM modelling

The main objective of this work is to advance stem cell modelling specifically and cell modelling in general. Therefore, we have systematically constructed a cellular biomechanical model by mathematically treating stem cells as soft matter.

From structural viewpoint, a cell consists of membrane wall, cytoplasm, microtubules, cell nucleus and cytoskeleton – cell's scaffold. The cell nucleus plays a central role in the response to mechanical forces (Caille et al. 2002). According to Maniotis et al. (1997), the nucleus inside the cell is about 9 times stiffer than the cytoplasm. Based on these observations, we propose to model the cell nucleus as hyperelastic material, which has been used in Caille et al. (2002) to model the nucleus of endothelia cells.

The cell membrane is basically a lipid bilayer. Up to date, the most successful cell model is the fluid mosaic model – the lipid bilayer model (Singer and Nicolson 1972). It captures two essential features of the lipid bilayer: fluidity and diffusion. A well-established and very successful mechanics or mathematics model for the cell membrane is Helfrich's liquid crystal cell membrane model (Helfrich 1973), which is based on or built on the fluid mosaic model. To extend Helfrich's liquid crystal membrane model, we propose to use a bulk nematic liquid crystal material to model the outer layer of the cells.

The rationale for such a soft matter physics cell model is that cell cytoplasm does not just consist of liquid, but it contains cell organelles and many weakly cross-linked polymer networks, such as actin filaments or intermediate filaments. Depending on the phenotype, the content, i.e. microstructure and the concentration, of these filaments may be different. In this work, we address the modelling of stem cells, which are of different types and may be in different stages. For certain stem cells, their structure may be still under development. According to Chowdhury et al. (2010), the embryonic stem cells are $\sim$ 10-fold softer than their differentiated counterparts. According to these observations, the cytoplasm region of our stem cell model contains a lower cytoskeleton component with a higher amount of liquid. Hence, the liquid crystal model becomes a suitable option for modelling our interpretation of cellular cytoplasm. For simplicity, in this preliminary two-layer cell model, we do not distinguish between the cell membrane and the cell cytoplasm. A refined soft matter physics model that distinguishes between the cell membrane and the cell cytoplasm will be reported in a follow-up paper.

Here, the ECM is modelled as a substrate consisting of a hyperelastic block, as used previously for both cell and gel models (see Fereol et al. 2009; Sen et al. 2009) (Figure 1). An illustration of the cell and the ECM model is shown in Figure 1.

In the following sections, we describe both the hyperelastic constitutive model and the liquid crystal model as applied in our cell–ECM modelling approach.

2.1 *Hyperelastic model*

The hyperelastic constitutive model is used to represent the intracellular scaffold and plasma aggregates, which are assumed to be isotropic and nonlinear, exhibiting an elastic response with large strains. There are more than 20

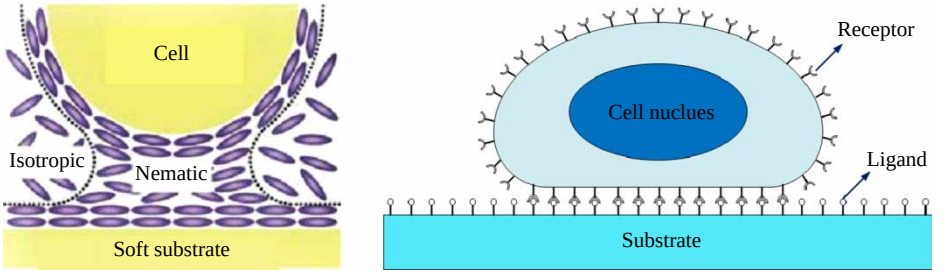

Figure 1. Soft matter cell model and soft adhesive contact model.

hyperelastic models for describing rubber-like materials, a comparison of different hyperelastic models can be found in Marckmann and Verron (2006). In our research, we adopted the modified Mooney–Rivlin material (Fried and Johnson 1988) to model the cell nucleus and ECM. The strain energy density function W for the modified Mooney–Rivlin material is given as

$$W = C_1\left(I_1 - 3I_3^{1/3}\right) + C_2\left(I_2 - 3I_3^{2/3}\right) + \frac{1}{2}\lambda(\ln I_3)^2, \quad (1)$$

where C_1, C_2 and λ are the material constants and $\mathbf{C} = \mathbf{F}^{\mathrm{T}} \cdot \mathbf{F}$ is the right Cauchy–Green deformation tensor; and the three invariants of the right Cauchy–Green tensor are defined as

$$I_1 = \mathrm{tr}(\mathbf{C}), \quad (2)$$

$$I_2 = \frac{1}{2}\left[(\mathrm{tr}(\mathbf{C}))^2 - \mathrm{tr}(\mathbf{C}^2)\right], \quad (3)$$

$$I_3 = \det(\mathbf{C}). \quad (4)$$

The corresponding constitutive relations can be expressed in terms of the second Piola–Kirchhoff stress tensor $\mathbf{S}$ and the invariants of the right Cauchy–Green tensor

$$\mathbf{S} = 2\{(C_1 + C_2 I_1)\mathbf{I} - C_2\mathbf{C} - \left(C_1 I_3^{1/3} + 2C_2 I_3^{2/3} - \lambda \ln I_3\right)\mathbf{C}^{-1}\}. \quad (5)$$

After the second Piola–Kirchhoff stress is obtained, the first Piola–Kirchhoff stress tensor can be immediately computed as $\mathbf{P} = \mathbf{S} \cdot \mathbf{F}^{\mathrm{T}}$, which can then be substituted into the later developed meshfree Galerkin formulation to calculate the internal nodal force.

If the substrate is modelled as a Mooney–Rivlin hyperelastic medium, its elastic stiffness tensor is a fourth-order tensor that can be expressed as

$$\mathbb{C} = 4\frac{\partial^2 W}{\partial \mathbf{C}\partial \mathbf{C}} = 4C_2\mathbf{I}\otimes\mathbf{I} + \frac{4}{3}\left(C_1 I_3^{1/3} + 4C_2 I_3^{2/3} - \lambda\right)\mathbf{C}^{-1}\otimes\mathbf{C}^{-1} - 4\left(C_1 I_3^{1/3} + 2C_2 I_3^{2/3} - \lambda \ln I_3\right)\mathbf{C}^{-1}\odot\mathbf{C}^{-1} - 4C_2\mathbb{I}. \quad (6)$$

By making the elastic constants, C_1, C_2 and λ, dependent on spatial coordinates, one can model the substrate with heterogeneous stiffness.

2.2 Liquid crystal cell model

Liquid crystals have biphasic properties by combining liquid and solid characteristics. For instance, a liquid crystal may be fluidic similar to a liquid, while having a long-range orientational order, and thus a solid elasticity was associated with deformations of the same order. There are many different types of liquid crystal phases (e.g. smectic, nematic and isotropic), which can be distinguished by their different optical properties (e.g. birefringence). Liquid crystal materials can mimic biological materials and systems; many biological systems including cell membranes, phospholipids, cholesterols and DNA exist in liquid crystal phases (see Stewart 2003; Stewart 2004; Woltman et al. 2007). In this cell modelling approach, we adopt a simplified version of the Ericksen–Leslie theory (Lin and Liu 2000) as the governing equations for the nematic liquid crystal component. The strong forms of the simplified Ericksen–Leslie theory are

$$\rho_0 \frac{D\mathbf{v}}{Dt} = \nabla \cdot \boldsymbol{\sigma} + \mathbf{b}, \quad \forall\, \mathbf{x} \in V(t), \quad (7)$$

$$\rho_0^d D\frac{\tilde{\mathbf{h}}}{Dt} = \gamma\{\nabla \cdot \nabla\otimes\mathbf{h} - \mathbf{r}(\mathbf{h})\}, \quad \forall\ \mathbf{x} \in V(t), \quad (8)$$

where $\mathbf{v}$ is the velocity field, $\mathbf{h}$ is the Nematic liquid crystal director field, $\mathbf{b}$ is the body force in the current configuration, ρ_0 and ρ_0^d are the density of fluid and director fields in the reference configuration, where the differential gradient operator is acting in the spatial configuration, i.e. $\nabla := (\partial/\partial x_i)\mathbf{e}_i$; γ is the director elastic constant, $\mathbf{r}$ is a Landau–Ginzburg type potential that governs the evolution of the director field

$$\mathbf{r} = \frac{\mathrm{d}R(\mathbf{h})}{\mathrm{d}\mathbf{h}} = \frac{\mathbf{h}}{\epsilon^2}\left(|\mathbf{h}|^2 - 1\right)$$

and

$$R(\mathbf{h}) = \frac{1}{4\epsilon^2}\left(|\mathbf{h}|^2 - 1\right)^2 \quad (9)$$

and the Cauchy stress is determined as

$$\sigma = -p\mathbf{I} + 2\mu\mathbf{d} - \eta\nabla\cdot(\nabla\otimes\mathbf{h}\odot\nabla\otimes\mathbf{h}) - \mathcal{G}. \quad (10)$$

In Equation (10), $p = \kappa(1 - J)$ is the hydrostatic pressure, κ is the bulk modulus, $J = \det(\mathbf{F})$, μ is viscosity and η is a positive constant.

3. Meshfree Galerkin formulation and the computational algorithm

A total Lagrangian formulation is developed for the soft matter cell model under finite deformation, and a Galerkin weak formulation is derived and used in the numerical computation. The numerical simulations are conducted by using meshfree methods (Li and Liu 2004). Meshfree methods have advantages in computing large deformation problems compared with traditional finite element method (FEM). In our meshfree simulation, both the cell and its substrate are discretised by a set of particles and then they are represented by meshfree interpolation functions.

The weak form of the balance of linear momentum under finite strain condition can be expressed as follows:

$$\sum_{i=1}^{2}\int_{\Omega_0^{(i)}}\rho_0^{(i)}\ddot{\mathbf{u}}^{(i)}\cdot\delta\mathbf{u}^{(i)}\,\mathrm{d}\Omega^{(i)}+\sum_{i=1}^{2}\int_{\Omega_0^{(i)}}\mathbf{P}^{(i)}:\delta\mathbf{F}^{(i)}\,\mathrm{d}\Omega^{(i)}=\sum_{i=1}^{2}\int_{\Omega_0^{(i)}}\rho_0^{(i)}\mathbf{B}^{(i)}\cdot\delta\mathbf{u}^{(i)}\,\mathrm{d}\Omega^{(i)}+\sum_{i=1}^{2}\int_{\Gamma_t^{(i)}}\bar{\mathbf{T}}^{(i)}\cdot\delta\mathbf{u}^{(i)}\,\mathrm{d}S^{(i)}+\sum_{i=1}^{2}\delta\Pi_{\mathrm{AC}}^{(i)},\tag{11}$$

where $\mathbf{B}$ is the body force, $\mathbf{P}$ is the first Piola–Kirchhoff stress, $\bar{\mathbf{T}}$ is the prescribed traction on the traction boundary $\Gamma_t^{(i)}$, $i=1$ corresponding to cell and $i=2$ corresponding to ECM substrate. Note that the last terms in Equation (11), $\delta\Pi_{\mathrm{AC}}^{(i)}$, denote the virtual work contribution from adhesive contact, which will be discussed in details in Section 4.

The nematic director evolution is only for cell, for simplicity, we do not introduce $i=1$ in the formulation, a weak form of the governing equation can be derived as

$$\begin{aligned}\int_{\Omega_0}\rho_0^d J\frac{D\mathbf{h}}{Dt}\cdot\delta\mathbf{h}\,\mathrm{d}\Omega=&-\int_{\Omega_0}\gamma\left\{(\mathbf{F}^{-1}\cdot\mathbf{F}^{-\mathrm{T}})\cdot(\nabla_X\otimes\mathbf{h})\right\}:(\nabla_X\otimes\delta\mathbf{h})\mathrm{d}\Omega\\&+\int_{\Gamma_t}\gamma\left\{\mathbf{N}\cdot(\mathbf{F}^{-1}\cdot\mathbf{F}^{-\mathrm{T}})\cdot(\nabla_X\otimes\mathbf{h})\right\}\cdot\delta\mathbf{h}\,\mathrm{d}S\\&+\int_{\Gamma_c}\gamma\left\{\mathbf{N}\cdot(\mathbf{F}^{-1}\cdot\mathbf{F}^{-\mathrm{T}})\cdot(\nabla_X\otimes\mathbf{h})\right\}\cdot\delta\mathbf{h}\,\mathrm{d}S\\&-\int_{\Omega_0}\gamma J\mathbf{r}(\mathbf{h})\cdot\delta\mathbf{h}\,\mathrm{d}\Omega,\end{aligned}\tag{12}$$

where Γ_c denotes the contact boundary. By assuming that

$$\mathbf{N}\cdot(\mathbf{F}^{-1}\cdot\mathbf{F}^{-\mathrm{T}})\cdot(\nabla_X\otimes\mathbf{h})\}=0,\quad\forall\mathbf{x}\in\Gamma_t$$

and

$$\mathbf{h}=\bar{\mathbf{h}}\Rightarrow\delta\mathbf{h}=0,\quad\forall\mathbf{x}\in\Gamma_c.$$

Consider the following meshfree interpolation:

$$\mathbf{u}(\mathbf{X},t)=\sum_{I=1}^{n_{\mathrm{node}}}N_I(\mathbf{X})\,\mathbf{d}_I(t),\tag{13}$$

$$\mathbf{h}(\mathbf{X},t)=\sum_{I=1}^{n_{\mathrm{node}}}N_I(\mathbf{X})\mathbf{h}_I(t).\tag{14}$$

Note that even though the director field, $\mathbf{h}(X,t)$, is essentially a part of displacement gradient, the robustness of meshfree computation allows us to use equal-order interpolation without causing severe numerical instability.

Following the standard meshfree discretisation procedure, e.g. Li and Liu (2004), we can obtain the following discrete equations of motion with the understanding that these equations of motions are applied to both the cell and the substrate:

$$\mathbf{M}\ddot{\mathbf{d}}=\mathbf{f}^{\mathrm{ext}}-\mathbf{f}^{\mathrm{int}}(\mathbf{d}),\tag{15}$$

where $\mathbf{M}$ is the lumped mass matrix, $\mathbf{f}^{\mathrm{int}}$ is the internal force array arising from the current state of stress and $\mathbf{f}^{\mathrm{ext}}$ is the external force array including body forces and surface traction and contact forces

$$\mathbf{M}_{IJ}=\int_{\Omega_0}\rho_0\mathbf{N}_I\mathbf{N}_J\,\mathrm{d}\Omega,\tag{16}$$

$$\mathbf{f}_I^{\mathrm{int}}=\int_{\Omega_0}P_{iJ}\mathbf{N}_{I,J}\mathbf{e}_i\,\mathrm{d}\Omega,\tag{17}$$

$$\mathbf{f}_I^{\mathrm{ext}}=\int_{\Omega_0}\rho_0\mathbf{B}_i\mathbf{N}_I\mathbf{e}_i\,\mathrm{d}\Omega+\int_{\Gamma_t}\bar{\mathbf{T}}_i\mathbf{N}_I\mathbf{e}_i\,\mathrm{d}S+\int_{\Gamma_c}\bar{\mathbf{f}}_i\mathbf{N}_I\mathbf{e}_i\,\mathrm{d}S.\tag{18}$$

At time $t_{n+1}=t_n+\Delta t$, the discrete equation of motion can be written as

$$\mathbf{M}\mathbf{a}_{n+1}=\mathbf{f}_{n+1}^{\mathrm{ext}}-\mathbf{f}_{n+1}^{\mathrm{int}}.\tag{19}$$

If the central difference scheme is used in the time integration, we have

$$\mathbf{d}_{n+1}=\mathbf{d}_n+\Delta t\mathbf{v}_n+\frac{1}{2}\Delta t^2\mathbf{a}_n,\tag{20}$$

$$\mathbf{a}_{n+1}=\mathbf{M}^{-1}\left(\mathbf{f}_{n+1}^{\mathrm{ext}}-\mathbf{f}_{n+1}^{\mathrm{int}}\right),\tag{21}$$

$$\mathbf{v}_{n+1}=\mathbf{v}_n+\frac{1}{2}\Delta t(\mathbf{a}_n+\mathbf{a}_{n+1}),\tag{22}$$

where $\mathbf{d}$, $\mathbf{a}$ and $\mathbf{v}$ denote the nodal displacement, acceleration and velocity arrays, respectively.

For the nematic liquid crystal, we can define the internal general force for director field as

$$\mathbf{f}_I^h=-\left\{\int_{\Omega_0}\mathcal{P}_{i,J}N_{I,J}(\mathbf{X})\mathbf{e}_i\,\mathrm{d}\Omega+\int_{\Omega_0}\gamma J\mathbf{r}_iN_I(\mathbf{X})\mathbf{e}_i\,\mathrm{d}\Omega\right\},\tag{23}$$

where the generalised internal force for the director field is defined as

$$\mathcal{P}=\gamma\left(\mathbf{F}^{-1}\cdot\mathbf{F}^{-\mathrm{T}}\right)\cdot(\nabla_X\otimes\mathbf{h}),\tag{24}$$

if the central difference scheme is used in time integration, we have

$$\mathbf{v}_{n+1}^h=\mathbf{M}_h^{-1}\mathbf{f}_{n+1}^h,\tag{25}$$

$$\mathbf{h}_{n+1}=\mathbf{h}_n+\Delta t\mathbf{v}_{n+1}^h.\tag{26}$$

4. Adhesive contact model for cell–substrate interactions

The interplay between a cell and its ECM is defined by complex interactions between ligands and receptors.

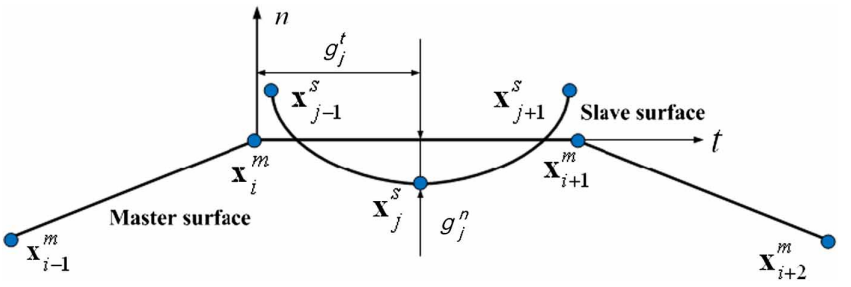

Figure 2. A penetrated slave particle and corresponding master segment.

In this research approach, we do not model the exact molecular mechanisms of the adhesion phenomenon or the detailed molecular motions during this complex process. Instead, we model an overall adhesion effect between cells and their substrates. The specific attractive adhesion force may be simulated by an attractive potential force, whereas the steric interaction between the cell membrane and the substrate is treated as the repulsive force.

We have developed a computational algorithm and modelling techniques to simulate cellular adhesive contact. The main features of this contact algorithm are (1) using the regular continuum contact mechanics to simulate a repulsive force and (2) using a postulated adhesive potential to mimic an attraction force. The continuum contact mechanics algorithm is illustrated in Figure 2. In the proposed adhesive contact algorithm, the adhesive force is modelled by a special potential force that is determined by the distance between a point on the cell membrane and its shortest distance to the substrate as described in Equation (28). In this case, we do not model the repulsive force, but adopt the conventional finite element or meshfree contact algorithm to enforce the impenetrable condition between the cell and its substrate.

By assuming that the density and the size of the substrate are much larger than the density and the size of the cell, we may neglect the direct adhesive force from the cell to the substrate. The total virtual work contribution from the adhesive contact force may be written as

$$\delta\Pi_{\mathrm{AC}} = \int_{\Omega_0} B(r)\frac{\mathbf{r}}{r}\cdot\delta\mathbf{u}\,\mathrm{d}\Omega + \int_{\Gamma_{\mathrm{c}}^{(1)}} \mathbf{f}^c\cdot\delta\mathbf{g}\,\mathrm{d}S, \qquad (27)$$

where the adhesive attraction force is modelled by the potential force

$$B(r) = G\,\mathrm{e}^{-r/d_0}, \qquad (28)$$

where G and d_0 are the constants and $\mathbf{r}$ is the position vector between nodal particles on the cell and the corresponding surface element of the substrate. For the adhesive contact, the membrane may be in contact with the ECM. During this process, inter-penetration of the cell membrane and the ECM surface is not permitted. The impenetrable condition is enforced to identify the repulsive force by using finite element-based continuum mechanics contact algorithm. Hence, the second integral in Equation (27) is a surface integral, in which $\mathbf{g}$ is the gap vector and $\mathbf{f}^c$ is being modelled as the repulsive normal force plus a contact frictional force.

The basic concept behind the classical contact procedure is that the two contacting bodies first penetrate into each other within a single explicit time integration step, while additional nodal forces are introduced into the contacting nodal points such that the impenetrability conditions are strictly enforced. We adopted the exact enforcement of the impenetrability condition in a single time step as previously described (Hughes et al. 1976).

In our contact simulations, both the cell and the ECM can be made deformable. Typically, the contacting surfaces are designated as 'master' and 'slave'. Here, we treated the cell's outer surface as the slave and the ECM substrate surface as the master.

The contact algorithm begins with prediction of the slave particles at time step n, the contact-detection algorithm is then used to search all the inter-penetration particles based on the determinant value of the meshfree moment matrix (Li et al. 2001). When all penetration points are detected, the next step is to calculate the normal gap and relative tangential velocity between the intrusion slave particles and the closest master surface locations (Figure 2). The procedures are outlined as follows:

(i) Calculate the normal (n) and tangential (t) gaps

$$g_j^n = (\mathbf{x}_j^s - \mathbf{x}_i^m)\cdot\mathbf{n}_i, \qquad (29)$$

$$g_j^t = (\mathbf{x}_j^s - \mathbf{x}_i^m)\cdot\mathbf{t}_i \qquad (30)$$

with

$$\mathbf{t}_i = \frac{(\mathbf{x}_{i+1}^m - \mathbf{x}_i^m)}{\|\mathbf{x}_{i+1}^m - \mathbf{x}_i^m\|}, \qquad (31)$$

$$\mathbf{n}_i = \mathbf{e}_3 \times \mathbf{t}_i, \qquad (32)$$

where $\mathbf{n}_i$ is the outward normal vector of the ith master segment matching with the jth penetrated slave particle and $\mathbf{e}_3$ is the unit vector pointing outward from the plane.

(ii) Calculate the normal and tangential forces

The contact force $\mathbf{f}^c$ has two components: the normal repulsive contact force and the tangential contact friction force. The normal direction repulsive force may be defined as

$$\mathbf{f}_j^n = \frac{2M_j^s g_j}{\Delta t^2}\mathbf{n}_i = f_j^n \mathbf{n}_i. \tag{33}$$

In the tangential direction, the classical Coulomb friction model is adopted in modelling the forces between the slave body and the master body. To enforce the stick or static condition, we have

$$\mathbf{f}_j^{\text{stick}} = -\frac{M_j^s}{\Delta t}\mathbf{v}_j^t. \tag{34}$$

The tangential force cannot exceed the force limit at which the interface can hold. After reaching the limit, a slip or dynamic condition should be applied

$$\mathbf{f}_j^{\text{slip}} = -\left|\mu_k f_j^n\right| \frac{\mathbf{v}_j^t}{\|\mathbf{v}_j^t\|}. \tag{35}$$

The tangential force is the minimum of these two forces or

$$\mathbf{f}_j^t = -\min\left(|\mu_k f_j^n|, \|\mathbf{f}_j^{\text{stick}}\|\right)\frac{\mathbf{v}_j^t}{\|\mathbf{v}_j^t\|}, \tag{36}$$

where μ_k is the friction coefficient which is dependent upon the two interacting surface materials and $\mathbf{v}_j^t$ is the relative tangential velocity between the j-th slave particle and the i-th master segment.

(iii) Update the contact force for each master contact particle

During the simulation, the substrate is deformable. Therefore, the contact force needs to be added to the master nodal particles to make sure that the total force is balanced. We use linear interpolation to distribute the contact forces of the two nodal particles to the corresponding master segment

$$\mathbf{f}_i^n = -(1-\alpha)\mathbf{f}_j^n, \tag{37}$$

$$\mathbf{f}_i^t = -(1-\alpha)\mathbf{f}_j^t, \tag{38}$$

$$\mathbf{f}_{i+1}^n = -\alpha\mathbf{f}_j^n, \tag{39}$$

$$\mathbf{f}_{i+1}^t = -\alpha\mathbf{f}_j^t, \tag{40}$$

where

$$\alpha = \frac{g_j^t}{\|\mathbf{x}_{i+1}^m - \mathbf{x}_i^m\|}, \quad (0 \le \alpha < 1). \tag{41}$$

(iv) Redistribute the contact forces to neighbouring particles within the substrate.

The nodal force vectors calculated above are the exact vectors for each penetrating slave particle and the corresponding master nodal surface particles. In the meshfree approach, we redistribute each exact nodal force to its supporting nodal particle. After the force redistribution, the contact force at a particle I becomes

$$\bar{\mathbf{f}}_I = \sum_{J=1}^{n_{\text{node}}} N_I(\mathbf{X}_J)\mathbf{f}_J. \tag{42}$$

In the FEM interpolation, $N_I(\mathbf{X}_J) = \delta_{IJ}$, we then recover the exact nodal force vector.

In this work, the interface between ligands and receptors is modelled as an interactive zone that separates the cell from the substrate, and the adhesive force distribution varies according to the magnitude of the gap distribution. The adhesive interaction is strong near the contact zone, and it decays as material points move away from the contact zone. The attractive component of the adhesive contact model is similar to a special version of the coarse-grain FEM adhesion contact algorithm as proposed for long-range van der Waals forces by Sauer and Li (2007).

5. Numerical simulations

As an application of soft matter physics and a multiscale contact-adhesion algorithm, we have uniquely simulated cell–ECM contact and adhesion mechanics. To ensure a meaningful simulation, we have first conducted a validation test of the proposed cell model. By doing so, we identified critical parameters of the soft matter model. We then applied the verified material model to simulate contact between a cell and various substrates with different stiffness. We have also simulated the interaction between a cell and a substrate with non-uniform stiffness. In addition, we also extended the current cell model to 3D.

5.1 Validation of the cell model

To validate the proposed cell model, we have applied it to simulate cell deformation under compression and compared with experiment measurements for endothelial cells (Caille et al. 2002). The constant force is applied at the top and bottom rigid microplates, and the boundary nodes are in contact with the cell surface. The classical contact algorithm is applied in the two contact surfaces. In the simulation, the cell deformation is defined as the relative reduction in height, i.e. $(H_0 - H)/H_0$. We first set the whole cell as hyperelastic Mooney–Rivlin material and fit the force–deformation curve (see Figure 3(c)) to get the material constants. Then, we put the fitted hyperelastic Mooney–Rivlin material in the cell nucleus, and outside of the nucleus region is modelled as nematic liquid crystal.

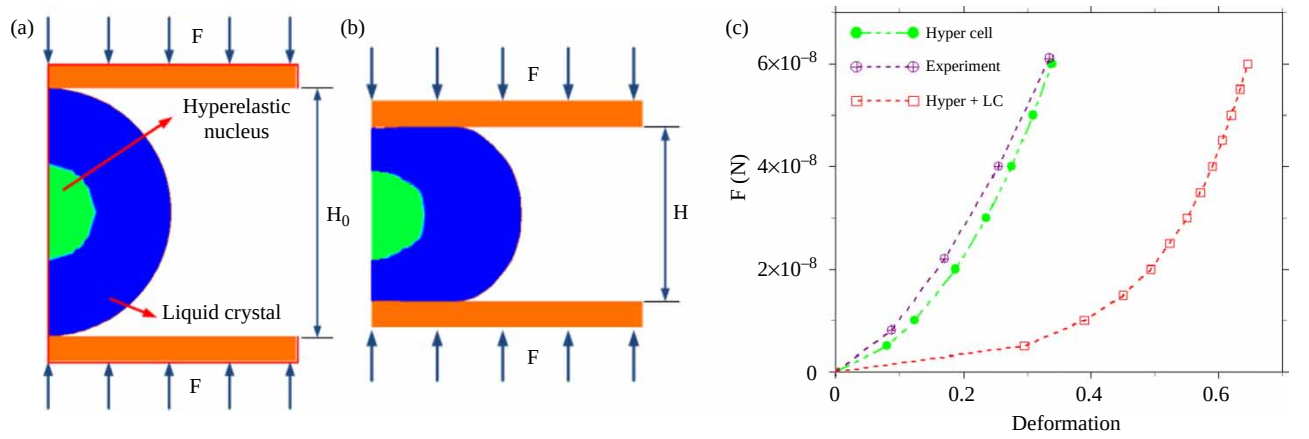

Figure 3. Validation of the cell model: (a) before deformation; (b) after deformation; (c) force–deformation curve.

Figure 3(a),(b) shows the cell shape before and after deformation. The force–deformation curve is plotted in Figure 3(c). The applied compressive forces increase nonlinearly as a function of the cell height reduction. From the simulation (see Figures 3(c) and 4), one can find that the force required to create the same deformation for endothelia cell is larger than the stem cells, which is reasonable considering that the stem cells are undeveloped cells. Because the two phenotypes are dramatically different, it is inaccurate to fit the stem cell model with the experimental data obtained from endothelial cells. As can be seen from Figure 3, our stem cell model is much softer than endothelial cells, which most likely is true in reality.

5.2 *Cell response in four different stiffness substrates*

The cell is modelled as a circular plate for 2D, with a diameter of $D = 10\,\mu\text{m}$. The substrate is modelled as a 2D plate with a dimension of ($L \times H = 39.78\,\mu\text{m} \times 4.5\,\mu\text{m}$). Plain strain is assumed in our simulations. The exact problem statement is shown in Figure 5.

In meshfree computation, a total of 4455 particles are used in discretisation of the cell, and 5525 particles are used to form the meshfree discretisation of the substrate. The nucleus of the cell is modelled as hyperelastic Mooney–Rivlin material. The initial density is $\rho^0 = 1.0\times 10^3\,\text{kg/m}^3$, and the material constants are $C_1^n = 2.126\times 10^3\,\text{Pa}$, $C_2^n = 1.700\times 10^2\,\text{Pa}$ and $\lambda^n = 1.700\times 10^5\,\text{Pa}$. The region beyond the hyperelastic nucleus is modelled as nematic liquid crystal. The density of the liquid crystal is chosen as $\rho^0 = 1.0\times 10^3\,\text{kg/m}^3$, the density of the director field is $\rho_d^0 = 1.0$ and the material properties and constants are $\kappa = 2.2\times 10^9\,\text{Pa}$, $\mu = 1.0\times 10^{-3}\,\text{kg/(m s)}$, $\eta = 5.0\times 10^{-8}$, $\varepsilon = 1.0\times 10^{-6}$ and $\gamma = 1.0\times 10^{-4}$.

The substrate is modelled as hyperelastic Mooney–Rivlin material. Four different substrates with different stiffness are considered. The density for the four substrates is the same as that of the cell nucleus. We set the material constants $C_1 = 1.265\times 10^4\,\text{Pa}$, $C_2 = 1.012\times 10^3\,\text{Pa}$ and $\lambda = 1.012\times 10^6\,\text{Pa}$. The material properties for four different substrates are chosen as

$$C_1^{S1} = C_1,\quad C_1^{S2} = 2C_1,\quad C_1^{S3} = 5C_1,\quad C_1^{S4} = 10C_1$$
$$C_2^{S1} = C_2,\quad C_2^{S2} = 2C_2,\quad C_2^{S3} = 5C_2,\quad C_2^{S4} = 10C_2$$
$$\lambda^{S1} = \lambda,\quad \lambda^{S2} = 2\lambda,\quad \lambda^{S3} = 5\lambda,\quad \lambda^{S4} = 10\lambda.$$

Initially, the cell stands still and the initial gap between the cell and the substrate is 200 nm. The bottom surface of

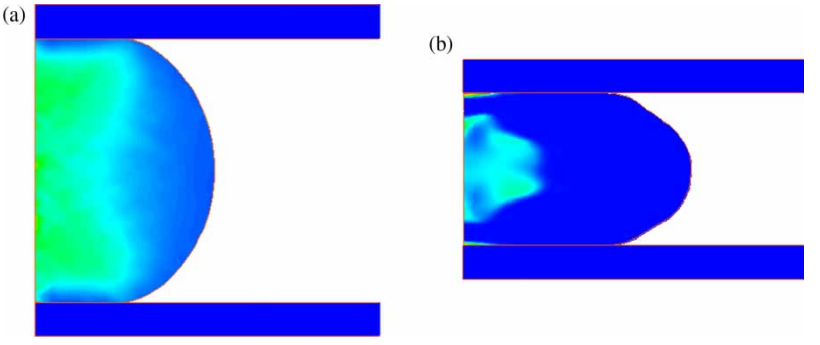

Figure 4. Deformation of the cell model under force $F = 3\times 10^{-8}\,\text{N}$: (a) hyperelastic cell; (b) liquid crystal cell with a hyperelastic nucleus.

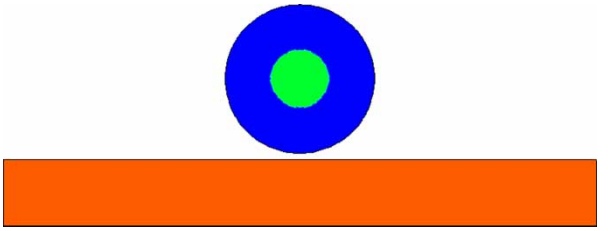

Figure 5. Computational model of cell spreading on different substrates (different colour stands for different material models).

the substrate is fixed during the whole simulation time. The adhesive force brings the cell into contact with the substrate, and then the cell spreads under the adhesive contact forces. The constants $G = 9.8 \times 10^6$ N/kg and $d_0 = 1.0 \times 10^{-5}$ m are chosen for the adhesive potential force. Simulations were carried out for cells in contact with four substrates of different elastic modulus (stiffness) described above.

From this simulation, one may observe the cell spreading over time. In Figure 6, we display the cell shapes and effective stress on four different substrates with different stiffness under the same contact conditions at the same time. One may find that the contact between the cell and the softest substrate (substrate I) (Figure 6 (a)) generates the least cell spreading, and the contact between the cell and substrate II (Figure 6(b)) has the second least spreading, the cell on the substrate III has the second most spreading (Figure 6(c)) and when the substrate stiffness is kept increasing, the cell on the substrate IV has the most spreading (Figure 6(d)).

It may be noted that although the case IV generates the most cell spreading, when we keep increasing the substrate stiffness, the difference becomes very small, which means the spreading may not increase any more when the stiffness of the substrate reaches a certain value. However, within certain range, cell spreading area is directly related to the stiffness of the substrate, and it is purely a phenomenon of soft elasticity. Based on this model, the stem cell is a mechanical sensor, and it can translate the mechanical information (properties) of the substrate into its shape, configuration and size. We have identified this as a strong evidence supporting cell mechanotransduction without incorporating the concept of 'tensegrity' on the structure of cell scaffold (Wang et al. 2009). In fact, embryonic stem cells do not have well-developed cell-scaffold structures. To the best of authors' knowledge, this type of cell response has not been previously reported.

Because this is a continuum simulation, one can measure the stress at every position of the cell. In Figure 7, we display computation results that have been carried out for cells in contact with 10 substrates with different elastic modulus (stiffness). We have sampled the effective stress at the centre of the cell nucleus at the same time instance. We then plot the magnitude of the effective stress vs. the different values of substrate stiffness. One can clearly observe that as the substrate stiffness increases the magnitude of the effective stress increases. Similar correlation has been observed in experimental measurement of contractile force of stem cells (e.g. Discher et al. 2005).

5.3 *Conformation change due to substrate elasticity*

The main rationale to use the liquid crystal model to simulate stem cells is its representation of weakly

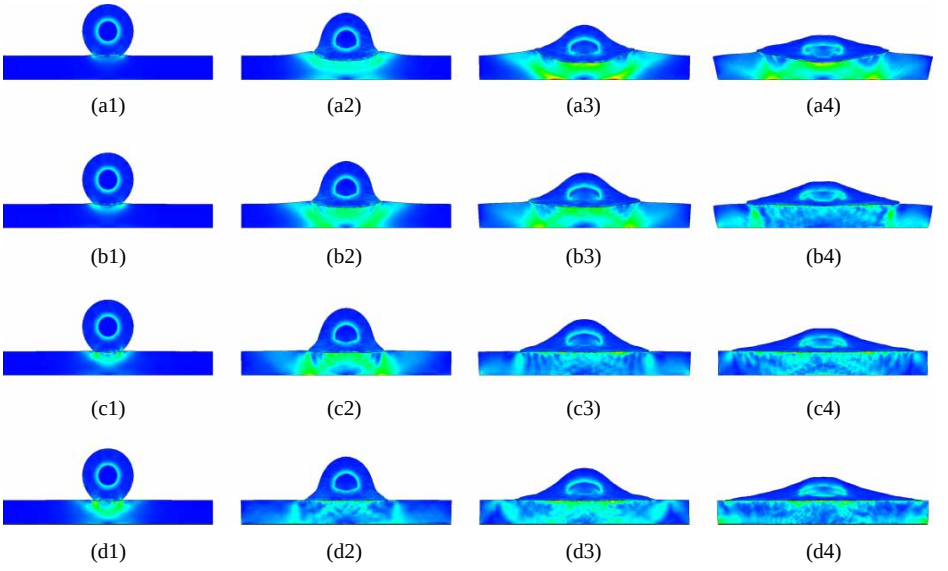

Figure 6. Cell spreading over substrates with different stiffness: (a) substrate I, (b) substrate II, (c) substrate III and (d) substrate IV.

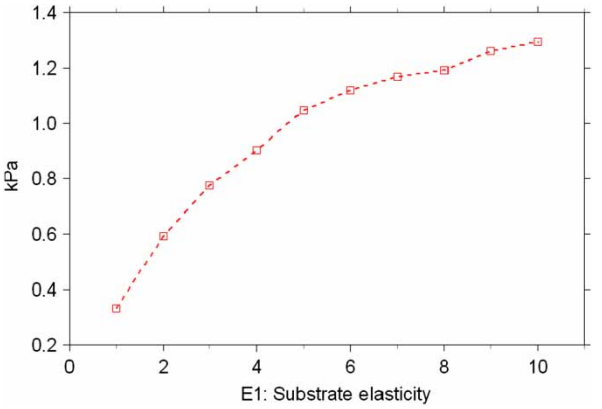

Figure 7. Effective stress vs. elastic stiffness of the substrate.

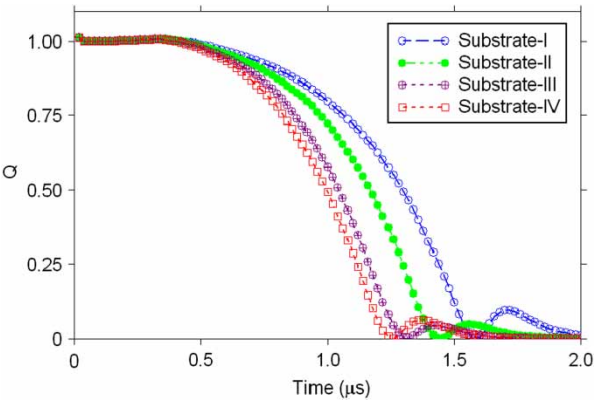

Figure 8. Order parameter evolution with time with respect to different substrates.

cross-linked hydrogel, which may serve as a model for undeveloped cross-linked actin filaments inside the cell before the polymerisation. The order parameter of a nematic director field, $\mathbf{Q}$, is a macroscopic tensorial field that may represent the statistical average of molecular orientation order or molecular conformation at a given point inside the cell.

We hypothesise that the molecular orientation order may be linked directly to protein expression and hence gene expression inside stem cells. It is thus meaningful to probe the relationship between the stiffness of the extracellular substrate and the nematic order parameter insider the cell. In literature of elastic theory of liquid crystals, the order parameter tensor is defined as a traceless tensor

$$\mathbf{Q} = \frac{3}{2}\mathbf{h}\otimes\mathbf{h} - \frac{1}{2}\mathbf{I}. \tag{43}$$

One may note that in Equation (43), the director field $\mathbf{h}$ is a unit vector, whereas in the Ericksen–Leslie theory, the strength of the director field may change due to diffusion or dissipation. Taking into account the effect of strength varying of the director field, $\mathbf{h}(\mathbf{X}, t)$, in this paper we adopt the following definition of order parameter:

$$\mathbf{Q} = \frac{3}{2}\mathbf{h}\otimes\mathbf{h} - \frac{|\mathbf{h}|^2}{2}\mathbf{I} = |\mathbf{h}|^2\left(\frac{3}{2}\hat{\mathbf{h}}\otimes\hat{\mathbf{h}} - \frac{1}{2}\mathbf{I}\right), \tag{44}$$

where

$$\hat{\mathbf{h}} := \frac{\mathbf{h}}{|\mathbf{h}|}.$$

In Figure 8, we display the effective order parameter

$$Q = \sqrt{\mathbf{Q} : \mathbf{Q}}$$

evolution histories for substrates with four different stiffness at a chosen sampling point near the initial contact zone. According to Figure 8, the order parameter measured on the substrate with the lowest elastic stiffness is on the top of those measured on the less stiff substrates. In fact, the order parameter evolution history curves descend as the elastic stiffness of the substrate increases. However, based on our calculations after certain time period of spreading, the effective order parameter on four different substrates converges to almost the same value. Based on this soft matter model, this may indicate that the mechanotransduction effect is time dependent, and it may be a dominant factor only at the early stage of stem cell differentiation process. After certain time, other factors may play more important roles in such a complex and well-coordinated physiology event.

5.4 *Cell response in a stiffness-varying substrate*

It is interesting to consider cell contact with substrate that has non-uniform stiffness. We set the material properties in the substrate as a function of position x to observe the cell spreading motion in different directions:

$$C_1^S = C_1(0.1 + 9.9r), \quad C_2^S = C_2(0.1 + 9.9r),$$
$$\lambda^S = \lambda(0.1 + 9.9r),$$

where r is defined as $r = (x + L/2)/L$ with the centre of the substrate at $x = 0$. The exact problem statement is

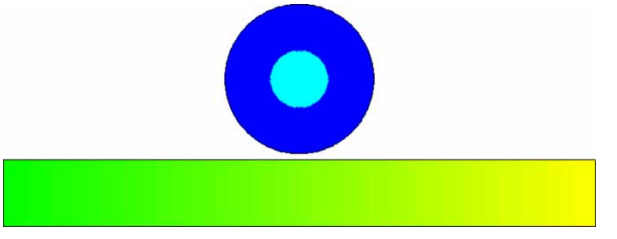

Figure 9. Computational model of cell spreading on a stiffness-varying substrate, the colour in the substrate stands for different stiffness, the stiffness at the right end is the highest.

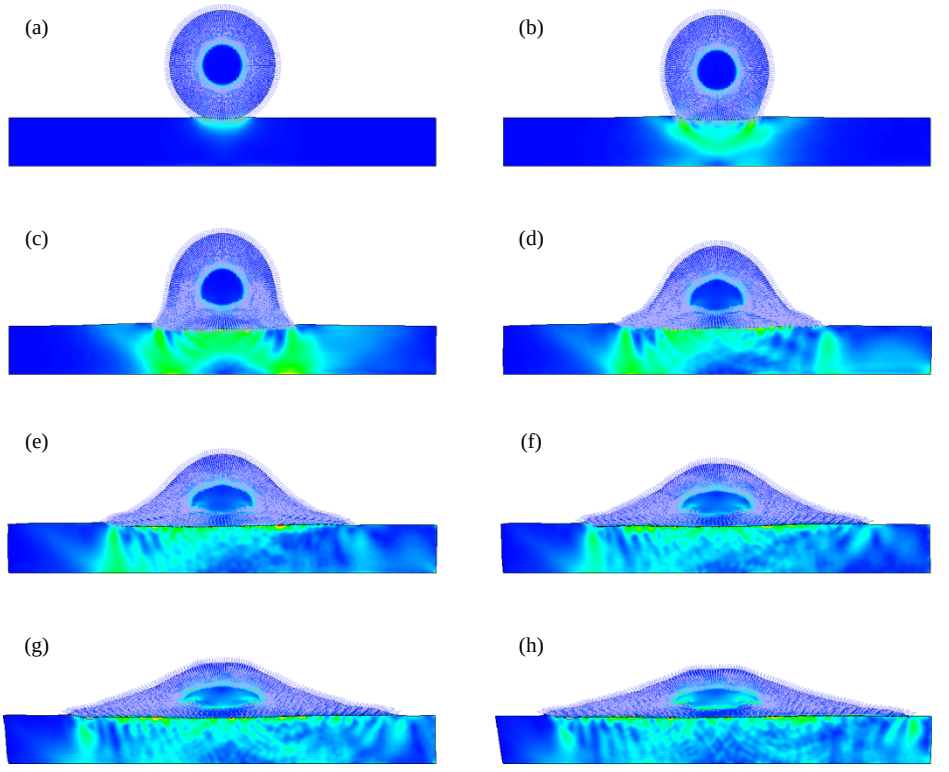

Figure 10. Time sequence of cell contact with a stiffness-varying substrate (stress contour with director field).

shown in Figure 9. In Figure 10, we display a time sequence of a cell contacting with a stiffness-varying deformable substrate. The colour contour is the effective stress contour. Without varying the stiffness, the cell should move equally on both the left and the right side of the substrate. From the simulation results, one can find immediately that cell move towards the right side much faster than to the left side of the substrate due to the stiffness gradient, which means that the cell is in favour of stiffer substrate. These results agreed well with experimental measurements (Wong et al. 2003; Engler et al. 2006) and numerical simulations (Ni and Chiang 2007) of cell adhesion and migration.

5.5 3D simulation of cell spreading

In the following simulations, the cell is modelled as a spherical ball in 3D, with a diameter of $D = 10\,\mu\text{m}$. The substrate is modelled as a 3D horizontal circular plate with a dimension of $R \times H = 15\,\mu\text{m} \times 5\,\mu\text{m}$. The cell nucleus in the 3D model is the same as in the 2D model. In the meshfree computation, a total of 4341 particles are used in discretising the cell and 16,640 particles are used to form the discretisation of the substrate. The nucleus of the cell is modelled as a hyperelastic Mooney–Rivlin material. In this original presentation, we have developed a 3D computational algorithm and modelling techniques to simulate the cell adhesive contacts.

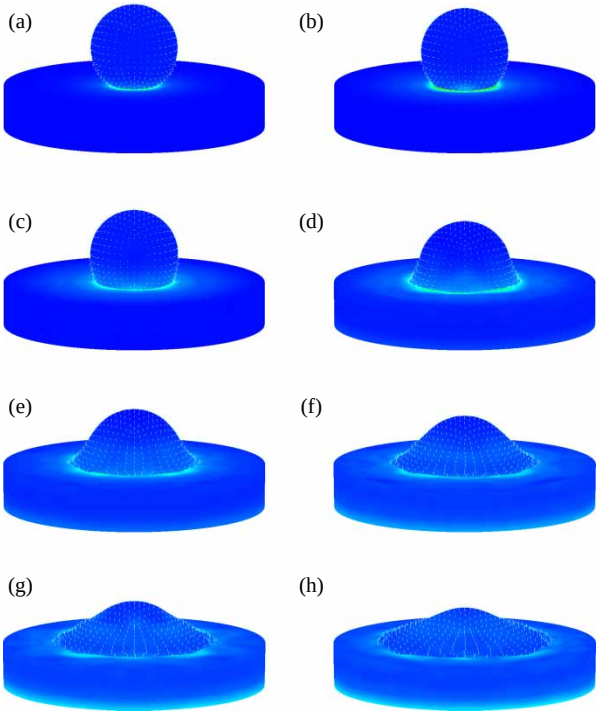

Figure 11. Time sequence of a 3D cell contact with a soft substrate (stress contour with director field).

Similar results have been observed from 3D simulations. In Figure 11, we display the time sequence of a cell contacting on a soft substrate. The colour contour is the effective stress and the white arrow represents the director field. Comparing with the 2D results, 3D simulations provide a possible way to capture the cell morphology changes as previously described in Ni and Chiang (2007).

6. Discussions and conclusions

To develop a fully 3D soft matter cell model that is capable of explaining cell adhesion, locomotion and its structure transformation coupled with focal adhesion is a challenging task. In this work, we extended the 2D cell model to 3D. The developed soft matter cell model for cell contact simulations may provide possible explanations on cell mechanotransduction and other issues at the large-scale level.

Our simulations have shown that (1) by using the proposed soft matter cell model, when a 'cell' is in contact with a substrate, the stress status in the cell may change depending on the stiffness of the substrate (see Figure 7); (2) the size of spreading area of the cell also changes or differs depending on the stiffness of extracellular substrate (see Figure 6) and (3) during soft contact process, the cell is in favour of stiffer substrate (see Figure 10). It should be noted that cell behaviour, in particular stem cell behaviour, is a complex biological phenomenon. The proposed soft matter cell model is only intended to model mechanical behaviours of cells at a coarse-gaining level, which may not and cannot explain the molecular mechanisms of cell motion, evolution and proliferation, and it requires an in-depth study of every aspects of molecular cell biology including all relevant biochemical, biophysical and biomechanical factors and their interactions at different scales.

Developing soft matter models for cells especially stem cells may help us understand biomechanical and biophysical behaviours of cells. It has been shown in this paper that the soft matter model can offer much more explanations on interaction between the stem cell and its mechanical niche than that of hyperelastic cell models or viscoelastic cell models. In some cases, the soft matter model has even shown its predictive power. It is the authors' opinion that by combining the soft matter cell model with molecular simulation, we may be able to achieve qualitative prediction on cell behaviours in collaborating with experimental observation. The predictive power of the stem cell model may provide both scientific insight and clinic guidance on a host of health care problems, such as regenerated medicine and drug design and delivery problems.

The soft matter cell model presented in this work is a primitive one, but it may open a door for more realistic and more accurate modelling of cells, especially stem cells. It is possible that along the line more sophisticated soft matter models can be developed, which are capable of simulating self-assembly of focal adhesion, cell division, proliferation and more.

Acknowledgements

This research was supported by the A. Richard Newton Research Breakthrough Award from Microsoft Corporation and a grant from National Science Foundation (CMMI No. 0800744). These supports are greatly appreciated.

References

Bao G, Suresh S. 2003. Cell and molecular mechanics of biological materials. Nat Mater. 2:715–725.

Caille N, Thoumine O, Tardy Y, Meister J. 2002. Contribution of the nucleus to the mechanical properties of endothelial cells. J Biomech. 35:177–187.

Chien S. 2007. Mechanotransduction and endothelial cell homeostasis: the wisdom of the cell. Am J Physiol Heart Circ Physiol. 292:H1209–H1224.

Chowdhury F, Na S, Li D, Poh Y-C, Tanaka TS, Wang F, Wang N. 2010. Material properties of the cell dictate stress-induced spreading and differentiation in embryonic stem cells. Nat Mater. 9:82–88.

Cuvelier D, Thery M, Chiu Y, Dufour S, Thiery J, Bornens M, Nassoy P, Mahadevan L. 2007. The universal dynamics of cell spreading. Curr Biol. 17:694–699.

Deshpande VS, Mrksich M, McMeeking RM, Evans AG. 2008. A bio-mechanical model for coupling cell contractility with focal adhesion formation. J Mech Phys Solids. 56: 1484–1510.

Discher DE, Janmey P, Wang YL. 2005. Tissue cells feel and respond to the stiffness of their substrate. Science. 310: 1139–1143.

Discher DE, Mooney DJ, Zandstra PW. 2009. Growth factirs, matrices, and forces combine and control stem cells. Science. 324:1673–1677.

Engler AJ, Sen S, Sweeney HL, Discher DE. 2006. Matrix elasticity directs stem cell lineage specification. Cell. 126: 677–689.

Fereol S, Fodil R, Laurent VM, Balland M, Louis B, Pelle G, Hnon S, Planus E, Isabey D. 2009. Prestress and adhesion site dynamics control cell sensitivity to extracellular stiffness. Biophys J. 96:2009–2022.

Freund LB, Lin Y. 2004. The role of binder mobility in spontaneous adhesive contact and implications for cell adhesion. J Mech Phys Solids. 52:2455–2472.

Fried I, Johnson AR. 1988. A note on elastic energy density functions for largely deformed compressible rubber solids. Comput Methods Appl Mech Eng. 69:53–64.

Geiger B, Spatz JP, Bershadsky AD. 2009. Environmental sensing through focal ashesions. Nat Rev Mol Cell Biol. 10: 21–33.

Helfrich W. 1973. Elastic properties of lipid bilayer: theory and possible experiments. Z Naturforsch C. 28:693–703.

Hughes TJR, Talor R, Sackman J, Curnier A, Kanoknukulchai W. 1976. A finite element method for a class of contact-impact problem. Comput Methods Appl Mech Eng. 8: 249–276.

Li S, Liu WK. 2004. Meshfree particle methods. Berlin: Springer.

Li S, Qian D, Liu WK, Belytschko T. 2001. A meshfree contact-detection algorithm. Comput Methods Appl Mech Eng. 190: 3271–3292.

Lin FH, Liu C. 2000. Existence of solutions for the Ericksen-Leslie system. Arch Rat Mech Anal. 154:135–156.

Liu P, Zhang YW, Cheng QH, Lu C. 2007. Simulations of the spreading of a vesicle on a substrate surface mediated by receptor-ligand binding. J Mech Phys Solids. 55:1166–1181.

Maniotis AJ, Chen CS, Ingber DE. 1997. Demonstration of mechanical connections between integrins, cytoskeletal filaments, and nucleoplasm that stabilize nuclear structure. Proc Natl Acad Sci USA. 94:849–854.

Marckmann G, Verron E. 2006. Comparison of hyperelastic models for rubberlike materials. Rubber Chem Technol. 79(5):835–858.

Ni Y, Chiang MYM. 2007. Cell morphology and migration linked to substrate rigidity. Soft Matter. 3:1285–1292.

Paszek MJ, Zahir N, Johnson KR, Lakins JN, Rozenberg GI, Gefen A, Reinhart-King CA, Margulies SS, Dembo M, Boettiger D et al., 2005. Tensional homeostasis and the malignant phenotype. Cancer Cell. 8:241–254.

Rehfelt F, Engler AJ, Eckhardt A, Ahmed F, Discher DE. 2007. Cell responses to the mechanochemical micro-environment – implications for regenerative medicine and drug delivery. Adv Drug Deliv Rev. 59:1329–1339.

Roy S, Qi HJ. 2010. A computational biomimetic study of cell crawling. Biomech Model Mechanobiol. 9:573–581.

Sauer R, Li S. 2007. A contact mechanics model for quasi-continua. Int J Numer Methods Eng. 71:931–962.

Sen S, Engler AJ, Discher DE. 2009. Matrix strains induced by cells: computing how far cells can feel. Cell Mol Bioeng. 2:39–48.

Singer SJ, Nicolson GL. 1972. The fluid mosaic model of the structure of cell membranes. Science. 175:720–731.

Stewart GT. 2003. Liquid crystals in biology – I. Historical, biological and medical aspects. Liquid Crystals. 30: 541–557.

Stewart GT. 2004. Liquid crystals in biology – II. Origins and processes of life. Liquid Crystals. 31:443–471.

Sun L, Cheng QH, Gao HJ, Zhang YW. 2009. Computational modeling for cell spreading on a substrate mediated by specific interactions, long-range recruiting interactions, and diffusion of binders. Phys Rev E. 79:061907.

Wang N, Tytell JD, Ingber DE. 2009. Mechanotransduction at a distance: mechanically coupling the extracellular matrix with the nucleus. Nat Rev Mol Cell Biol. 10:75–82.

Winer JP, Oake S, Janmey PA. 2009. Non-linear elasticity of extracellular matrices enables contractile cells to communicate local position and orientation. PLoS ONE. 4(7):e6382.

Woltman SJ, Jay GD, Crawford GP. 2007. Liquid-crystal materials find a new order in biomedical applications. Nat Mater. 6:929–938.

Wong JY, Velasco A, Rajagopalan P, Pham Q. 2003. Directed movement of vascular smooth muscle cells on gradient-compliant hydrogels. Langmuir. 19:1908–1913.

Yeung T, Georges PC, Flanagan LA, Marg B, Ortiz M, Funaki M, Zahir N, Ming W, Weaver V, Janmey PA. 2005. Effects of substrate stiffness on cell morphology, cytoskeletal structure, and adhesion. Cell Motil Cytoskelet. 60:24–34.

Zeng X, Li S. 2011. Multiscale modeling and simulation of soft adhesion and contact of stem cells. J Mech Behav Biomed Mater. 4:180–189.